# A Calibrated Blade-Element/Momentum Theory Aerodynamic Model of the MARIN Stock Wind Turbine

## Preprint

A. Goupee
*University of Maine*

R. Kimball
*Maine Maritime Academy*

E.-J. de Ridder and J. Helder
*Maritime Research Institute Netherlands*

A. Robertson and J. Jonkman
*National Renewable Energy Laboratory*

*To be presented at the International Society of Offshore and Polar Engineers Conference (ISOPE 2015)*
*Kona, Hawaii*
*June 21–26, 2015*

**NREL is a national laboratory of the U.S. Department of Energy**
**Office of Energy Efficiency & Renewable Energy**
**Operated by the Alliance for Sustainable Energy, LLC**

This report is available at no cost from the National Renewable Energy Laboratory (NREL) at www.nrel.gov/publications.

**Conference Paper**
NREL/CP-5000-63568
April 2015

Contract No. DE-AC36-08GO28308

**NOTICE**



This report is available at no cost from the National Renewable Energy Laboratory (NREL) at www.nrel.gov/publications.

Available electronically at http://www.osti.gov/scitech

Available for a processing fee to U.S. Department of Energy and its contractors, in paper, from:

U.S. Department of Energy
Office of Scientific and Technical Information
P.O. Box 62
Oak Ridge, TN 37831-0062
phone: 865.576.8401
fax: 865.576.5728
email: mailto:reports@adonis.osti.gov

Available for sale to the public, in paper, from:

U.S. Department of Commerce
National Technical Information Service
5285 Port Royal Road
Springfield, VA 22161
phone: 800.553.6847
fax: 703.605.6900
email: orders@ntis.fedworld.gov
online ordering: http://www.ntis.gov/help/ordermethods.aspx

*Cover Photos: (left to right) photo by Pat Corkery, NREL 16416, photo from SunEdison, NREL 17423, photo by Pat Corkery, NREL 16560, photo by Dennis Schroeder, NREL 17613, photo by Dean Armstrong, NREL 17436, photo by Pat Corkery, NREL 17721.*

# A Calibrated Blade-Element/Momentum Theory Aerodynamic Model of the MARIN Stock Wind Turbine

*Andrew J. Goupee*
University of Maine
Orono, Maine, USA

*Richard W. Kimball*
Maine Maritime Academy
Castine, Maine, USA

*Erik-Jan de Ridder*
Maritime Research Institute Netherlands
Wageningen, The Netherlands

*Joop Helder*
Maritime Research Institute Netherlands
Wageningen, The Netherlands

*Amy N. Robertson*
National Renewable Energy Laboratory
Golden, Colorado, USA

*Jason M. Jonkman*
National Renewable Energy Laboratory
Golden, Colorado, USA

## ABSTRACT

In this paper, a calibrated blade-element/momentum theory aerodynamic model of the Maritime Research Institute Netherlands (MARIN) stock wind turbine is developed and documented. The model is created using open-source software and calibrated to closely emulate experimental data obtained by the DeepCwind Consortium using a genetic algorithm optimization routine. The provided model will be useful for those interested in validating floating wind turbine numerical simulators that rely on experiments utilizing the MARIN stock wind turbine—for example, the International Energy Agency Wind Task 30's Offshore Code Comparison Collaboration Continued, with Correlation project.

KEY WORDS: MARIN stock wind turbine; floating wind turbine; blade-element/momentum theory; genetic algorithm; numerical model calibration

## INTRODUCTION

In recent years, the University of Maine, Maine Maritime Academy, the National Renewable Energy Laboratory (NREL), and the Maritime Research Institute Netherlands (MARIN) have worked toward developing wind turbine designs for the purpose of conducting model-scale, coupled wind/wave basin tests of floating wind turbines that mimic their full-scale physics (Fowler et al., 2013; Kimball et al., 2014; Martin et al., 2014). In 2013, MARIN put these methods into practice and devised an improved, performance-matched wind turbine dubbed the MARIN stock wind turbine (MSWT) (de Ridder et al., 2014). This $1/50^{th}$-scale performance-matched wind turbine is capable of generating appropriately scaled aerodynamic thrust forces under low-Reynolds number, Froude-scaled winds (no small feat) to emulate the full-scale NREL 5-MW reference wind turbine. In addition, the power (and torque) generated by the improved model wind turbine is much closer to the full-scale equivalent than the geometrically-scaled wind turbine tested in 2011 (see Martin et al., 2014) by these parties and is capable of using realistic blade-pitch controls. This design is achieved through the careful use of low-Reynolds number-specific airfoil sections in combination with slightly larger chord lengths (de Ridder et al., 2014).

During the past 2 years, the MSWT turbine has been used in several model test campaigns at MARIN. One example is the retesting of the OC4-DeepCwind semisubmersible to produce data for the validation of coupled aero-hydro-servo-elastic floating wind turbine simulators, including for use in Phase II of the International Energy Agency Wind Task 30's Offshore Code Comparison Collaboration Continued, with Correlation (OC5) project (Goupee et al., 2014). With the OC5 project in mind, this paper aims to create and document a description of the MSWT suitable for developing a model of the turbine in codes employing blade-element/momentum (BEM) theory or other actuator-line methods. This paper provides details on the creation of the base aerodynamic properties of the blade airfoil sections and the parameterization and tuning of the blade lift and drag coefficients with a genetic algorithm optimizer to best match data from several fixed-base tests of the MSWT. Tuning is necessary because of various factors—for example, uncertainties in rotational augmentation. The obtained model is shown to correlate well with experimental data for power and thrust values ranging over operational collective blade-pitch angles from 0° to 30° and tip-speed ratios ($TSR$s) from 2 to nearly 8. The final aerodynamic model is documented in this paper with sufficient detail for researchers to build a numerical model of the system.

## BLADE GEOMETRY

In this section, the geometry of the three-bladed, horizontal-axis MSWT required for performing aerodynamic calculations is presented. First, the radial distribution of the blade geometric properties is given. Afterword, the airfoil geometries for the blade are presented. It is important to note prior to discussing these details that the MSWT rotor has zero shaft tilt, zero blade precone, and that all blades are straight. That stated, readers should also keep in mind that in this and all subsequent sections, any results requiring units will be presented at full scale, not model scale. Details on the scaling laws used for this $1/50^{th}$-scale model can be found in Martin et al., (2014). Regarding blade structural details, which are not the focus here, it is worth mentioning that the blades were rigid for all practical purposes because of several pragmatic and scaling-related reasons (see Martin et al., 2014).

## Distributed Properties

The distributed properties of interest for performing aerodynamic calculations with a standard BEM theory method (see Manwell et al., 2009) include aerodynamic twist, chord length, and airfoil designation. It is important to note that the distributed properties to be provided assume a hub radius of 1.5 m and a tip radius of 63 m. The actual distributed properties for the blade can be found in Kimball et al. (2014) and are also given in Table 1.

Table 1. Distributed geometry properties for the MSWT

| Radius (m) | Twist (°) | Chord (m) | Airfoil Type (As Built/As Modeled) | Thickness (%) |
|---|---|---|---|---|
| 1.500 | 50.377 | 3.500 | Cylinder/Cylinder | 100.0 |
| 2.898 | 42.712 | 4.410 | Cylinder/Cylinder | 100.0 |
| 5.607 | 31.187 | 5.229 | Blend 1/Cylinder | 40.1 |
| 8.316 | 23.109 | 5.581 | Blend 2/AG04 Mod | 18.3 |
| 11.781 | 16.389 | 5.794 | Blend 3/AG04 Mod | 14.6 |
| 15.876 | 11.475 | 5.796 | Blend 4/AG04 Mod | 13.3 |
| 19.971 | 8.502 | 5.576 | Blend 5/AG04 Mod | 12.8 |
| 24.066 | 6.523 | 5.297 | AG04 Mod | 12.6 |
| 28.161 | 5.052 | 5.006 | AG04 Mod | 12.6 |
| 32.256 | 3.878 | 4.706 | AG04 Mod | 12.6 |
| 36.351 | 2.939 | 4.392 | AG04 Mod | 12.6 |
| 40.446 | 2.216 | 4.078 | AG04 Mod | 12.6 |
| 44.541 | 1.673 | 3.775 | AG04 Mod | 12.6 |
| 48.636 | 1.245 | 3.480 | AG04 Mod | 12.6 |
| 52.731 | 0.844 | 3.190 | AG04 Mod | 12.6 |
| 56.196 | 0.497 | 2.914 | AG04 Mod | 12.6 |
| 58.905 | 0.235 | 2.651 | AG04 Mod | 12.6 |
| 61.614 | 0.064 | 1.747 | AG04 Mod | 12.6 |
| 63.000 | 0.000 | 0.050 | AG04 Mod | 12.6 |

In Table 1, a 0° aerodynamic twist indicates that the chord line of the airfoil lies in the rotor plane (i.e., perpendicular to the incoming wind direction), with larger twists corresponding to trailing edges that move downwind relative to the leading edges. The blade-pitch angle, which will be used later in this work, effectively adds or subtracts to the aerodynamic twist uniformly throughout the entire length of the blade (for example, a 5° blade-pitch angle would place the second to last section noted in Table 1 at an effective twist of 5.064°).

As shown in the table, the MSWT was designed to use predominantly one airfoil shape, with the exception of the blade root that had to be blended to mate with a cylindrical hub connection. This was done primarily for simplicity. With the exception of the three stations nearest the root of the blade, the thickness of the blended airfoils is not much greater than that of the primary airfoil for the blade, this being a MARIN-modified Drela AG04 (AG04 Mod). As such, for the purposes of simplifying the numerical model of the blade and limiting the optimization of lift and drag coefficients to only one airfoil, the inner three sections of the blade will be modeled with zero-lift, drag-only cylindrical sections, and the remaining sections will utilize the aerodynamic properties of the modified Drela AG04 airfoil. This is also reflected in Table 1.

## Airfoil Geometry

Similar to the distributed properties, the two-dimensional airfoil geometry was also provided by Kimball et al. (2014). As noted earlier, the airfoil data for this geometry was employed for all sections, excepting the three inner stations that were assumed circular, for aerodynamic analyses. The resulting airfoil coordinates were normalized by the chord length $C$ of the airfoil section and are plotted in Fig. 1 for the 12.6% thick section. As evident from the figure, the airfoil is not very thick and possesses a small amount of camber. The complete set of normalized planar coordinates for the airfoil can be found in Kimball et al. (2014).

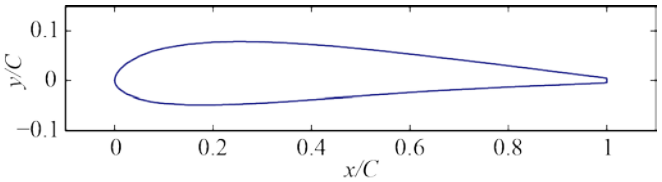


Fig. 1. Geometry of the MARIN-modified Drela AG04 airfoil

## GENERATION OF INITIAL AIRFOIL COEFFICIENTS

Initial airfoil lift and drag coefficients were required for the cylinder and airfoil as a basis for follow-on numerical modeling, including the aerodynamic tuning process. Pitching moment coefficients were ignored throughout the process and are not included in the final model.

For the cylinder, the lift coefficient, $C_L$, was taken as 0.0, and the drag coefficient, $C_D$, was assumed to be 0.5. Because these coefficients correspond to only a small portion of the blade near the root, their impact on aerodynamic performance of the rotor is minimal, and therefore no effort was made to calibrate them; thus, these values remained constant throughout the tuning process, and as such they are the same in the final calibrated model.

To begin estimating the lift and drag coefficients for the airfoil shown in Fig. 1, an analysis using XFOIL (Drela, 1989) was performed. XFOIL is a high-order panel code that incorporates a coupled viscous/inviscid interaction method designed specifically for airfoil analysis. The analysis was performed at a Reynolds number of 39,000, because this value is representative of the Reynolds number based on the chord length at 70% of the blade radius for conditions experienced during model testing. The analysis also employed a standard laminar-to-transition effect log factor, $N_{crit}$, of 9 (Drela and Giles, 1987). The angles of attack, $\alpha$, included in the analysis ranged from -5° to the stall point at 6°. The obtained lift and drag coefficients were then extrapolated over the entire possible range of angles of attack (-180° to 180°) using the NREL's AirfoilPrep tool (Hansen, 2012). An aspect ratio of 7.95 was used for this calculation. Rotational augmentation was also applied using this tool over the stalled region of the airfoil assuming a position of 70% of the blade. After smoothing the resulting coefficient curves using a fine division of $\alpha$ and MATLAB's interp1 function with the shape-preserving piecewise cubic interpolation method (pchip) selected, the initial lift and drag curves shown in Fig. 2 were obtained for use at all stations modeled as airfoils.

To demonstrate the need for aerodynamic tuning, these cylinder and airfoil coefficients were combined with the distributed properties shown in Table 1 and analyzed using BEM theory for the purposes of generating a comparison between the simulation and test data. NREL's WT_Perf was utilized as the BEM tool (Buhl Jr., 2004). This tool is very similar to the AeroDyn (Moriarty and Hansen, 2005) code used to compute the aerodynamic forces in NREL's popular floating wind turbine simulator, FAST (Jonkman and Buhl Jr., 2005). The simulation and test data results are expressed in terms of the power coefficient, $C_P$, and thrust coefficient, $C_T$, which are calculated as follows:

$$C_P = \frac{P}{1/2\,\rho A U^3}, \quad C_T = \frac{T}{1/2\,\rho A U^2}, \tag{1}$$

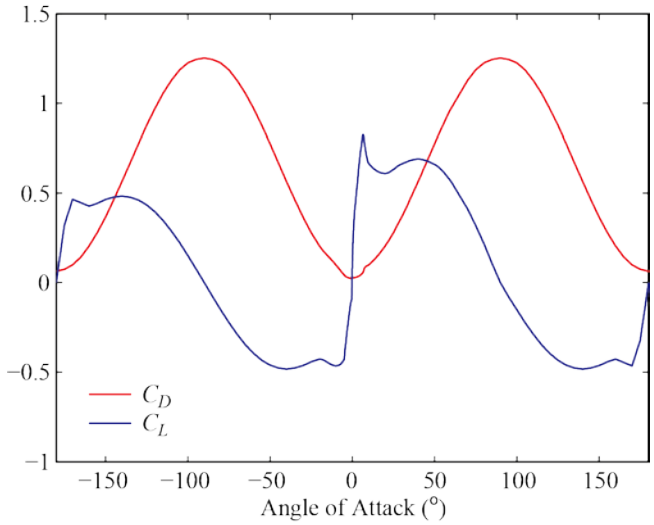


Fig. 2. Initial lift and drag coefficients for the modified AG04 airfoil

where $P$ is rotor power, $T$ is rotor thrust, $\rho$ is the density of air (1.225 kg/m$^3$), $A$ is the rotor swept area (12,469 m$^2$), and $U$ is the freestream wind speed normal to the rotor plane. The results are computed at multiple rotor speeds that are expressed in nondimensional fashion as a $TSR$. The $TSR$ is computed as:

$$TSR = \frac{\omega R}{U}, \tag{2}$$

where $\omega$ is the rotational speed of the rotor (in rad/s), and $R$ is the radius of the rotor. The simulation and test data are compared for two collective blade-pitch angles, $\theta$: 1° and 15°. Recall that as $\theta$ increases, the blade gains what is essentially a uniform increase in aerodynamic twist over the entire blade length relative to the 0° configuration shown in Table 1. The comparison of the various power and thrust coefficient curves is shown in Fig. 3.

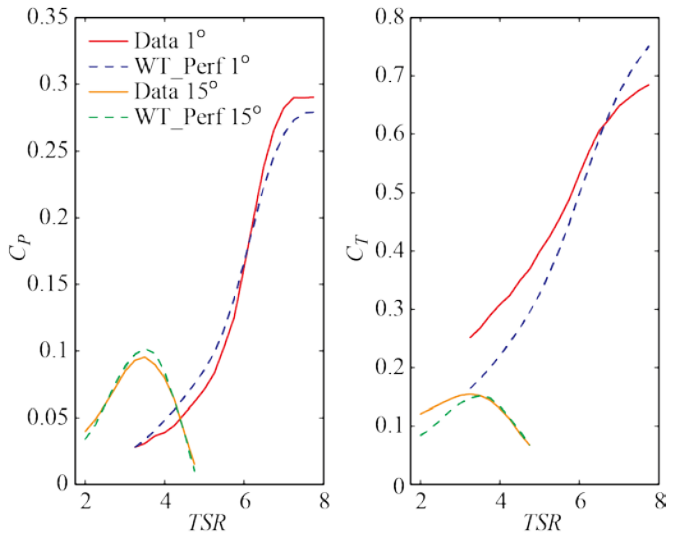


Fig. 3. Comparison of WT_Perf analysis using initial airfoil coefficients and test data for $C_P$ and $C_T$ over various $TSR$ for $\theta$ = 1° and 15°

As shown in Fig. 3, in general the comparison is fair, particularly for $C_P$; however, the prediction of $C_T$ is less than ideal. In particular, the $C_T$ curve predicted by WT_Perf is much steeper than the test data reported for the 1° case, and this configuration was heavily used in scenarios representing the rated wind speed condition during the May 2013 OC4-DeepCwind semisubmersible testing campaign. Because the thrust is the primary aerodynamic force produced by the wind turbine that influences global motion, it is imperative that a better correlation between the simulation results and test data be achieved. To facilitate better comparisons for code calibration work for floating wind turbine numerical tools such as FAST, the airfoil lift and drag coefficients require tuning to better capture the values and slopes of the $C_P$ and $C_T$ curves from the test data.

## TUNING OF AIRFOIL COEFFICIENTS TO MATCH EXPERIMENTAL DATA

In this section, the manner in which the airfoil coefficients are calibrated for the MSWT is presented. First, the parameterization of the airfoil coefficients in preparation for tuning is discussed. Subsequently, the formulation of an optimization problem for the purposes of finding the calibrated coefficients is described. Last, an overview of the algorithm used to execute the optimization problem is given.

### Parameterization of Airfoil Coefficients

Prior to outlining the parameterization, the initial lift coefficient curve is adjusted to obtain a simpler starting point. Specifically, the oddly shaped region after stall (6°) in the initial coefficients was eliminated in favor of a constant lift coefficient from stall to approximately 30°, equal to the value at stall and then blended to match the original coefficient value at 50°. Because this region is simply a deep-stall extension in AirfoilPrep with little physical justification, the change to a simpler curve is not unreasonable. In addition, the shape of the lift curve from -5° to stall produced by XFOIL possessed some significant variations in slope. Because these features seem undesirable, this portion of the lift coefficient curve is replaced by a straight line from the predicted -5° lift coefficient value to the stall point. This type of behavior is more representative of what basic theory predicts (i.e., flat plate lift) and will also facilitate needing fewer variables for tuning. Once the alterations are complete, the lift coefficient curve is transformed as shown in Fig. 4.

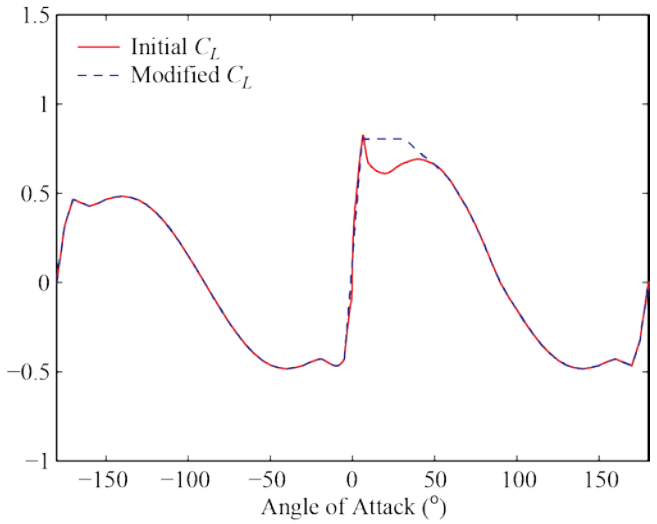


Fig. 4. Comparison of initial lift coefficient and modified coefficient to be used as the baseline for tuning

With the base lift and drag coefficients in hand, a method for parameterizing the curves for the purposes of tuning was established.

For efficient tuning, the number of design variables should be kept small; however, sufficient flexibility is required in the design space such that a reasonably good fit to the wind turbine test data can be obtained from the calibrated simulation. With this in mind, a set of variables was created following the methods of Bak and Fuglsang (2004) that would modify the values of the lift and drag curves at discrete angles of attack. The amount of the change to be applied at the angles of attack between these variables was determined through Matlab's interp1 function with the pchip method selected.

The locations of these variables for both the lift and drag coefficients were $\alpha$ = -5°, 6°, 12°, 18°, 24°, and 30°. This yielded 12 design variables in total. For angles of attack less than -5°, the change from the base configuration was interpolated using the aforementioned interpolation methods between $\alpha$ = -90° and -5°, with the change from the base configuration at -90° always equal to zero. Similarly, the change from the base configuration for $\alpha$ greater than 30° was performed from 30° to 90°, with the change at 90° always equal to zero. No change from the base coefficients occurred between 90° and -90° degrees angle of attack. The tuning point locations are shown in Fig. 5.

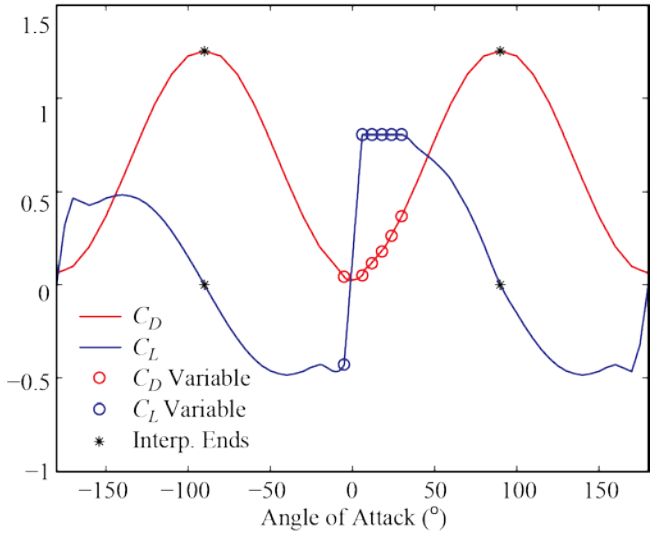


Fig. 5. Locations of the tuning variables and interpolation endpoints used in the aerodynamic tuning process

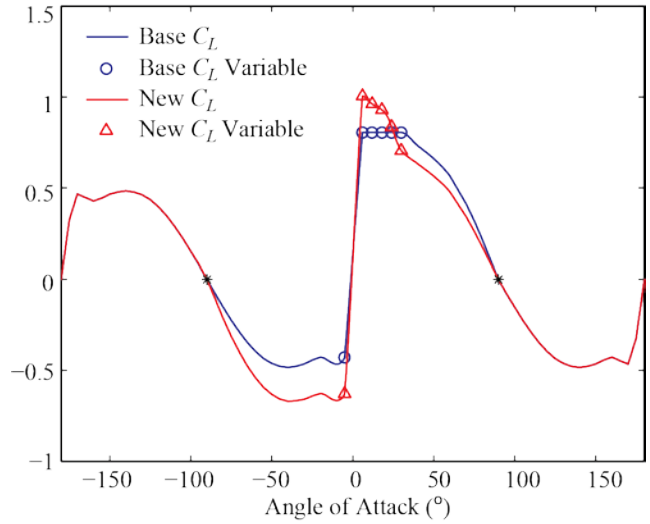


Fig. 6. Depiction of how airfoil coefficient variables can alter the lift (or, similarly, drag) coefficient curve

To better illustrate the process, an example of the alteration in the coefficient curve stemming from a set of nonzero tuning variables is given in Fig. 6. (The variables are set to nonzero arbitrarily for illustrative purposes only.) The figure, which shows both the base and altered (new) configurations, illustrates how the variables can shift the curves up or down at the selected locations and also visually demonstrates the interpolation process.

**Formulation of the Optimization Problem for Obtaining Calibrated Airfoil Coefficients**

In this subsection, the formulation of the optimization problem for the purposes of tuning the airfoil lift and drag coefficients such that simulations yield good comparisons with test data is discussed. The problem is formulated as a multiobjective optimization, in particular a bi-objective optimization. The first objective seeks to minimize the error between the $C_P(TSR)$ curves from the simulation and test data, whereas the second seeks to minimize the error between the $C_T(TSR)$ curves from simulation and test data (these objectives are not ordered in terms of priority). This is done as it is possible to achieve a good fit for the thrust coefficient response while simultaneously obtaining a poor prediction of the power coefficient if one chooses to calibrate the model based solely on matching experimental thrust data. Using a multiobjective formulation provides a set of Pareto-optimal solutions (Pareto, 1971) from which to choose where each solution possesses the lowest $C_P$ error for a given $C_T$ error (and vice versa). Once the Pareto-optimal solutions are obtained, one can select from the set of possible configurations based on higher-level engineering decisions—for example, the "realism" of the corresponding airfoil lift and drag coefficient curves.

To continue the problem formulation, the definition of several pertinent quantities is first presented. The tuning variables for the lift and drag curves are written as

$$\Delta C_{LD}^{(i)}, \quad i = 1,2,\dots,12, \tag{3}$$

where $\Delta C_{LD}^{(i)}$ is the change in value from the base configuration for either the lift ($i$ = 1, 2,…, 6) or drag ($i$ = 7, 8, …, 12) coefficient at the location corresponding to the $i^{\text{th}}$ variable. The mapping between $i$ and the angle of attack location is shown in Table 2.

Table 2. Mapping of variable index to angle of attack location

| $i$ | 1, 7 | 2, 8 | 3, 9 | 4, 10 | 5, 11 | 6, 12 |
|---|---|---|---|---|---|---|
| $\alpha$ (°) | -5 | 6 | 12 | 18 | 24 | 30 |

Next, the objective functions used in the optimization algorithm are defined. Because the intent is to match both the power and thrust coefficient behavior over a wide range of $TSR$s and collective blade-pitch angles, the objective functions utilize test results for several $TSR$s and two distinct $\theta$ values. The collective blade-pitch angles included in the objective functions are $\theta$ = 1° and 15°. The former was chosen because this was the blade-pitch angle setting employed for the May 2013 OC4-DeepCwind semisubmersible tests in the basin associated with near-rated wind speeds (13 m/s). The latter blade-pitch angle was chosen because it was the closest blade-pitch angle studied in wind turbine performance testing matching the blade-pitch setting used in the post-rated wind speed tests (17.2° for 21 m/s winds). The entire range of $TSR$ values obtained from testing were included in the objective functions: from 3.25 to 7.75 for the 1° setting and from 2 to 4.75 for the 15° setting. Although this arrangement includes a fair amount of data in the objective functions, 82% of the wind-only turbine

performance data remains for validation of the final calibrated model. All this noted, the objective functions $f_1$ and $f_2$ are computed as

$$f_1\left(\Delta C_{LD}^{(i)}\right) = \frac{100\%}{2}\left[\frac{\int_{3.25}^{7.75}\left|C_P^{D1}-C_P^{S1}\right|dTSR}{\max\left(C_P^{D1}\right)\int_{3.25}^{7.75}dTSR} + \frac{\int_{2}^{4.75}\left|C_P^{D15}-C_P^{S15}\right|dTSR}{\max\left(C_P^{D15}\right)\int_{2}^{4.75}dTSR}\right]$$
$$f_2\left(\Delta C_{LD}^{(i)}\right) = \frac{100\%}{2}\left[\frac{\int_{3.25}^{7.75}\left|C_T^{D1}-C_T^{S1}\right|dTSR}{\max\left(C_T^{D1}\right)\int_{3.25}^{7.75}dTSR} + \frac{\int_{2}^{4.75}\left|C_T^{D15}-C_T^{S15}\right|dTSR}{\max\left(C_T^{D15}\right)\int_{2}^{4.75}dTSR}\right] \quad (4)$$

where $C_P^{D1}$ is the power coefficient data for $\theta = 1°$, $C_P^{S1}$ is the power coefficient from simulation for $\theta = 1°$, $C_P^{D15}$ is the power coefficient data for $\theta = 15°$, $C_P^{S15}$ is the power coefficient from the simulation for $\theta = 15°$, $C_T^{D1}$ is the thrust coefficient data for $\theta = 1°$, $C_T^{S1}$ is the thrust coefficient from the simulation for $\theta = 1°$, $C_T^{D15}$ is the thrust coefficient data for $\theta = 15°$, and $C_T^{S15}$ is the thrust coefficient from the simulation for $\theta = 15°$. In simpler terms, the objective functions in Eq. 4 are essentially the average error over the investigated $TSR$ range normalized by the maximum value in the data and expressed as a percentage. Because each function utilizes two separate curves, the final result is the average of the normalized error for the two curves. Last, it should be noted that all simulation results in Eq. 4 were obtained with NREL's WT_Perf tool.

With the objective functions established, the optimization problem statement can be constructed. The optimization problem, including the constraints used, is as follows:

$$\begin{aligned} &\text{Find} && \Delta C_{LD}^{(i)}, \quad i = 1,2,\dots,12 \\ &\text{Minimize} && f_j\left(\Delta C_{LD}^{(i)}\right), \quad j = 1,2 \\ &\text{Subject to} && -0.2 \le \Delta C_{LD}^{(i)} \le 0.2, \quad i = 1,2,\dots,12 \\ & && C_D(\alpha) \ge 0.5 C_D^{Base}(\alpha), \quad -180° \le \alpha \le 180° \end{aligned} \quad (5)$$

where $C_D^{Base}$ is the drag coefficient for the unaltered, base configuration. This last constraint in Eq. 5 is enforced after the drag curve has been modified by the values in $\Delta C_{LD}^{(i)}$, and any drag coefficients less than $0.5C_D^{Base}$ are set equal to $0.5C_D^{Base}$. This permits the algorithm to explore lower drag coefficient options while preventing nonphysical $C_D$ that are extremely low or, even worse, less than or equal to 0.

**Multiobjective Genetic Algorithm**

To conduct the optimization problem posed in Eq. 5, a multiobjective genetic algorithm was employed. Genetic algorithms are a search-and-optimization technique that mimics the evolutionary principles and chromosomal processing in natural genetics. Genetic algorithms perform well in situations in which classical gradient-based algorithms often falter—for example, in the face of numerous design variables, nonlinear constraints, gradients that are difficult to compute, or multimodal objective functions that have several local minima. In addition, multiobjective genetic algorithms can provide an entire set of Pareto-optimal solutions with little to no additional computational time relative to a single-objective optimization unlike standard gradient-based methods.

For this particular aerodynamic tuning problem, a real-coded elitist nondominated sorting genetic algorithm (NSGA-II) was utilized (Deb et al., 2002). The details of the specific NSGA-II implementation used here are described in Goupee and Vel (2007). The particular settings for the algorithm are given in Table 3. Further information about the purpose of these parameters can be found in Goupee and Vel (2007).

Table 3. Parameter settings employed in the NSGA-II algorithm

| | |
|---|---|
| Population Size | 240 |
| Number of Genes | 12 |
| Number of Generations | 100 |
| Probability of Crossover | 1 |
| Probability of Crossover per Gene | 0.5 |
| Simulated Binary Crossover Strength Parameter | 2 |
| Probability of Mutation | 0.1 |
| Probability of Mutation per Gene | 0.5 |
| Polynomial-Based Mutation Strength Parameter | 2 |

## RESULTS

In this section, the results of the aerodynamic tuning for the MSWT are presented. First, the set of Pareto-optimal solutions is shown in the objective space and a specific solution for the tuning is selected based on engineering judgment. The calibrated airfoil characteristics are presented for the chosen solution in addition to the quality of the $C_P(TSR)$ and $C_T(TSR)$ curve fits between the calibrated simulations and data. Last, simulation results using the calibrated aerodynamics performed over multiple collective blade-pitch angles and $TSR$ values are compared to experimental data to assess the ability of the calibrated aerodynamic model to capture wind turbine performance in regions outside of the calibration region.

**Calibrated Solution**

Upon completion of the genetic algorithm optimization run, a set of Pareto-optimal solutions for the aerodynamic tuning were found, each possessing the minimum value of the first objective function, $f_1$, for a given value of the second objective function, $f_2$. The majority of the solutions in the objective space are displayed in Fig. 7.

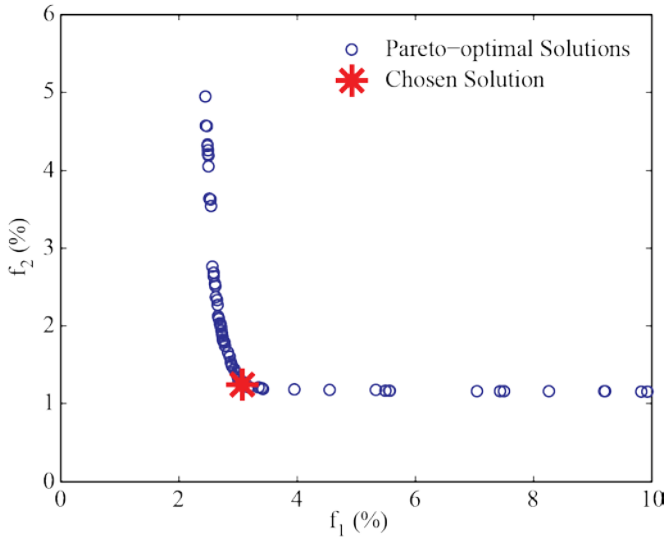


Fig. 7. Set of Pareto-optimal solutions for tuning the aerodynamics of the MSWT

With the set of aerodynamic tunings in hand from Fig. 7, a particular solution must be selected as the final tuning. As shown in the Pareto-front, major reductions in the power coefficient objective ($f_1$) can be made at a very minor expense in the thrust coefficient fit ($f_2$) until $f_1$ reaches below 4%. However, as the power coefficient objective is decreased from approximately 3% down toward 2%, the thrust coefficient objective is increased greatly from slightly more than 1% to

greater than 5%. And because matching the aerodynamics that best capture thrust is most critical, selecting a tuning that sacrifices some power prediction to better match the thrust response is desired. Therefore, a solution near the "knee" of the Pareto-front is selected with a slight preference for a tuning that provides a better relative fit for the thrust. In addition, the chosen solution, which is highlighted in Fig. 7, yielded lift and drag coefficient curves that appeared physically plausible with no significant kinks or odd behaviors. The lift and drag curves for the chosen calibrated aerodynamic solution are shown in Fig. 8.

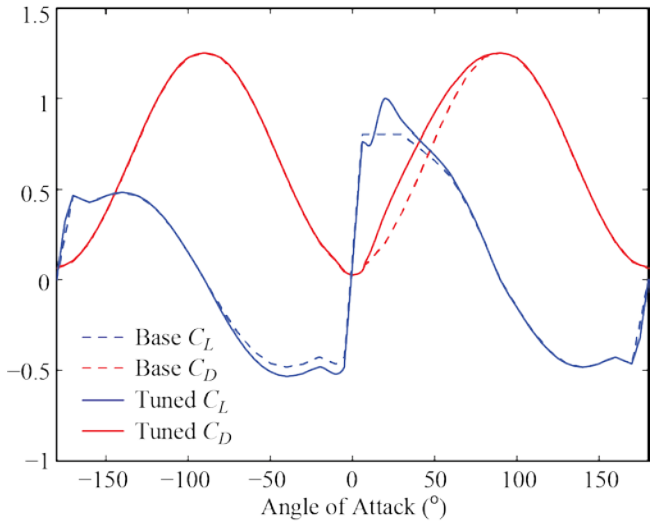


Fig. 8. Comparison of the base to calibrated lift and drag coefficients

Comparing the base to the calibrated solutions, it is found that the major deviations occur after stall (> 6°). The calibrated solution exhibits regions with both lower and higher lift coefficients post-stall, whereas the drag coefficient is consistently higher for the calibrated solution than the base solution beyond stall. Because the initial post-stall region aerodynamic coefficients were established based on simplistic extrapolations, it is not surprising that these regions of the calibrated solution possess the largest deviations from the base configuration.

To demonstrate that the calibrated solutions are sensible, but also to further emphasize the need for tuning, a comparison of the calibrated lift and drag coefficients to XFOIL predictions for angles of attack between -5° and 30° is shown in Fig. 9. In the figure, the XFOIL values from angles of attack from 6° to 30° were newly generated for this comparison alone and have not been altered using AirfoilPrep. That noted, both cases shown in the figure exhibit a slight dip in the post-stall lift followed by an increase beyond the stall lift coefficient. However, the XFOIL and calibrated $C_L$ deviate from each other past a 20° angle of attack. As for the drag coefficient, the calibrated solution exhibits smaller values until it reaches a little past 10°, beyond which the calibrated solution increases at a significantly faster rate than the XFOIL predictions. In short, Fig. 9. illustrates that the calibrated solutions are not far from the XFOIL prediction for small and modest angles of attack, but that larger angles of attack require significant corrections for BEM calculations to best match the test data.

Utilizing the calibrated aerodynamics shown in Fig. 8 in the analysis of the MSWT with WT_Perf yields the results shown in Fig. 10. As shown, the error between the predicted and measured thrust coefficient curves for both the $\theta$ = 1° and 15° collective blade-pitch settings is very slight throughout the entire range of $TSR$s investigated, and an excellent correlation between simulation and experiment has been achieved. In addition, although the fit is not as good as the thrust coefficient behavior, the match between the power coefficient curves from the simulation and test data is quite decent and better than the results obtained for the simulations using the initial airfoil coefficients shown in Fig. 3.

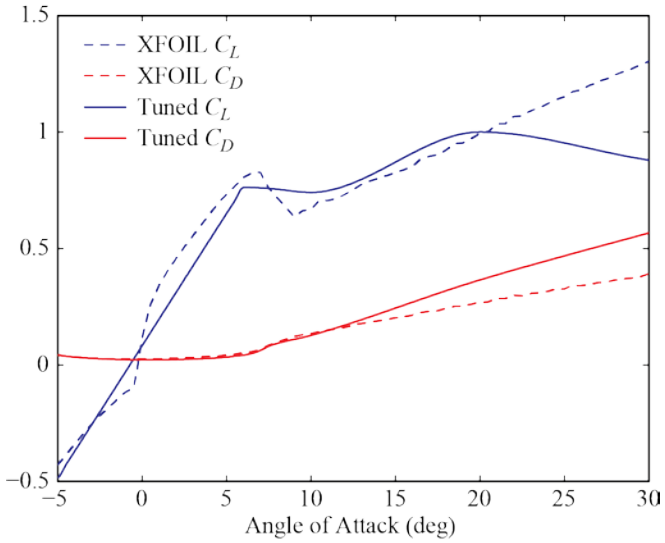


Fig. 9. Comparison of XFOIL and calibrated lift and drag coefficients for small to modest angles of attack

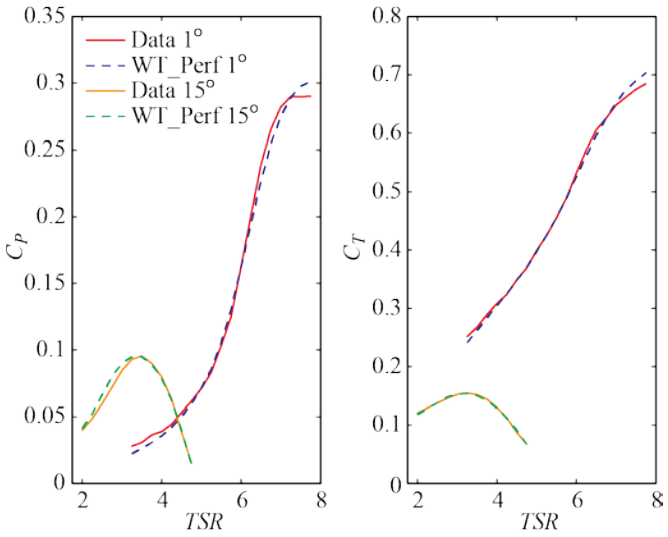


Fig. 10. Comparison of WT_Perf analysis using calibrated airfoil coefficients and test data for $C_P$ and $C_T$ over various $TSR$s for $\theta$ = 1° and 15°

To complete the documentation of the calibrated airfoil aerodynamics, the newly obtained lift behavior over small angles was inserted into NREL's AirfoilPrep to generate AeroDyn-style dynamic stall parameters, and an AeroDyn airfoil data input file was created. This file can be found in Appendix A. In addition, Appendix A contains the airfoil data input file for the cylindrical section used near the root of the blade.

**Performance of Calibrated Solution over Multiple Blade-Pitch Angles**

To complete the assessment of the calibrated aerodynamics for use in a broader range of operating conditions than those of interest here, WT_Perf simulations were performed for other blade-pitch settings for which model test data also existed. These additional angles included $\theta$ = 0°, 2°, 3°, 4°, 5°, 10°, 20°, 25°, and 30°.

Upon completion of the additional simulations, the results for the power coefficient, $C_P$, and thrust coefficient, $C_T$, predicted by WT_Perf for the collective additional blade-pitch angles in addition to the original angles used in the optimization were plotted against the experimental data over a range of $TSR$s. The results for the collective blade-pitch angles from 0° to 5° are shown in Figs. 11 and 12, and the comparison for the angles from 10° to 30° are shown in Figs. 13 and 14.

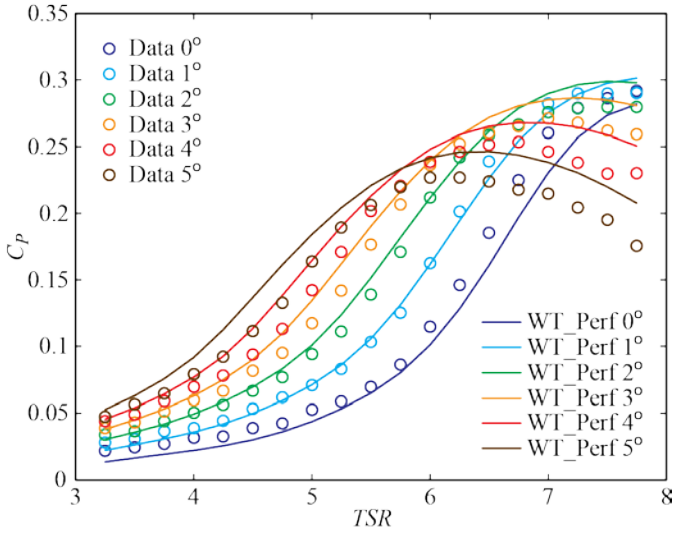


Fig. 11. Comparison of WT_Perf analysis using calibrated airfoil coefficients and test data for $C_P$ over various $TSR$ for $\theta$ = 0° to 5°

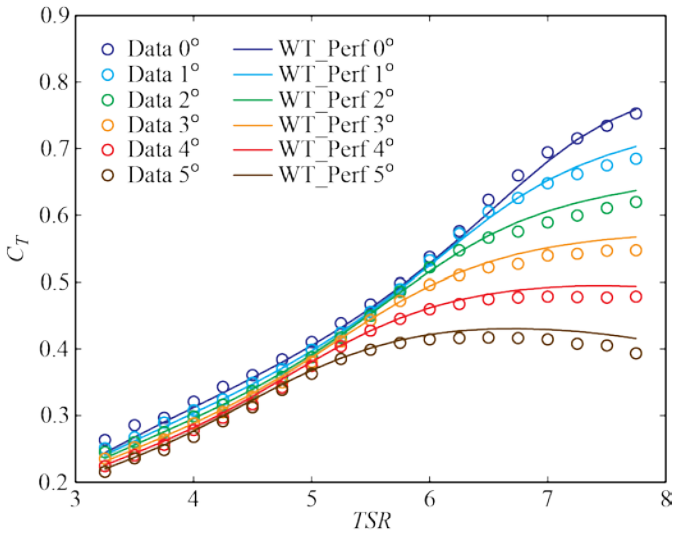


Fig. 12. Comparison of WT_Perf analysis using calibrated airfoil coefficients and test data for $C_T$ over various $TSR$ for $\theta$ = 0° to 5°

Examining the results for the shallower blade angles—i.e., $\theta$ = 0° to 5°—it is found that the best fit for $C_P$ between the simulation and test data is for $\theta$ = 1°. For the lone angle less than 1°, the calibrated simulation underpredicts the power coefficient over the range of $TSR$ investigated, whereas for $\theta$ > 1°, the calibrated simulation generally overpredicts $C_P$. A better fit can be found for the $C_T$ comparison shown in Fig. 12. In general, for all the smaller collective blade-pitch angles considered, the calibrated simulation accurately predicts the thrust coefficient. This is a desirable outcome, because the thrust force is the primary aerodynamic driver for global motions of floating wind turbines. This indicates that the calibrated aerodynamic model should be able to reliably predict the correct aerodynamic thrust loads when these pitch angles are in use, typically in near-rated and below-rated wind speed conditions. The power predictions corresponding to these operational parameters will generally be best at $\theta$ = 1° and will deteriorate slightly as the collective blade-pitch setting is altered from this position.

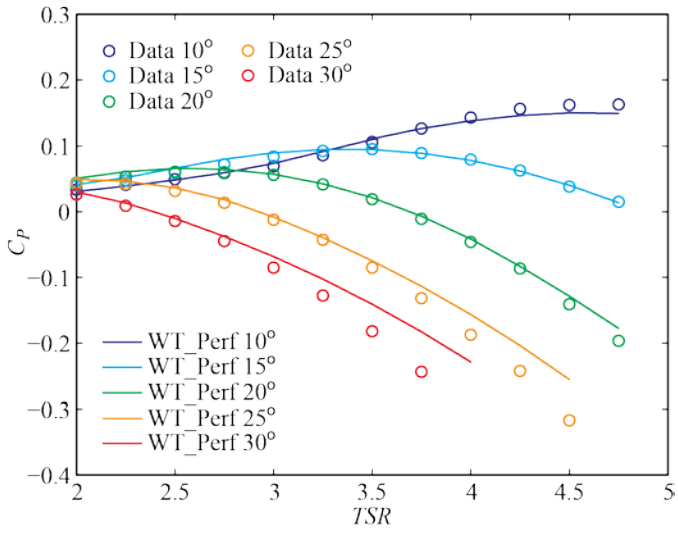


Fig 13. Comparison of WT_Perf analysis using calibrated airfoil coefficients and test data for $C_P$ over various $TSR$ for $\theta$ = 10° to 30°

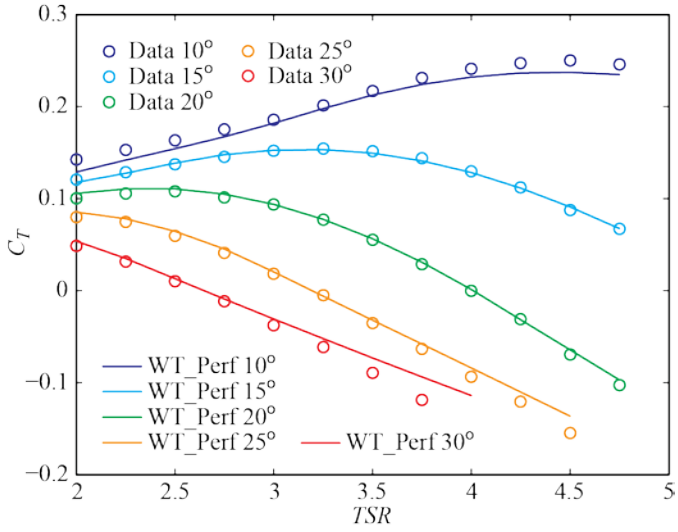


Fig 14. Comparison of WT_Perf analysis using calibrated airfoil coefficients and test data for $C_T$ over various $TSR$ for $\theta$ = 10° to 30°

Moving to the comparisons shown in Figs. 13 and 14 for collective blade-pitch angles between 10° and 30°, it is found that the calibrated simulation typically performs well in regard to matching the power and thrust coefficients observed from experiments. There are some moderate discrepancies in situations when either $C_P$ or $C_T$ is less than 0; however, these do not constitute regions of interest, because a turbine operating in these areas would not typically be modeled or simulated. In general, the calibrated aerodynamic model appears to capture the proper aerodynamic load behavior for the larger collective blade-pitch angles that might typically be found in post-rated wind speed operational conditions.

## CONCLUSIONS

To enable future numerical code validation efforts that utilize floating wind turbine model test data incorporating the MSWT, this paper creates and documents an aerodynamic model that captures the experimentally measured performance of the wind turbine as measured by the University of Maine, Maine Maritime Academy, and MARIN in May 2013. The geometry for the MSWT, which included airfoil section data as well as distributed chord and aerodynamic twist distribution data, was extracted from MARIN-sourced information documented in scientific literature. The airfoil lift and drag coefficients, which were initially created with the freely available codes XFOIL and AirfoilPrep, were parameterized to permit tailoring of the coefficients by altering values at discrete points between angles of attack from -5° to 30°. Using a multiobjective genetic algorithm to manipulate the tuning variables, the error between the power and thrust coefficients predicted by simulations using NREL's WT_Perf and measured data at selected operating points was minimized to create a calibrated aerodynamic model compatible with NREL's FAST and WT_Perf software and similar tools. Upon completion of the tuning process, the aerodynamic model was compared to test data for a wide range of nondimensional rotor speeds and collective blade-pitch angles and found to compare well to experimental observation. The calibrated aerodynamic model performed best at predicting the power coefficient for the collective blade-pitch angles of 1° and 15° as simulations and data corresponding to these angles were used in the calibration process. That noted, the power coefficient predictions from the simulator do not degrade significantly as the collective blade-pitch angle deviates from the aforementioned values. More importantly, the thrust coefficients, which characterize the most important aerodynamic load produced by a wind turbine that influences the global motion response of a floating wind system, are captured well by the calibrated aerodynamic model for all $TSR$s and collective blade-pitch angles investigated. Overall, the aerodynamic model contained in this paper should prove adequate for simulating the behavior of the MSWT throughout a wide range of conditions.

## ACKNOWLEDGEMENTS

The financial support from the U.S. Department of Energy through DeepCwind Grants DE-EE0002981 and DEEE0003728, the National Science Foundation through Grant IIP-0917974, and the University of Maine is gratefully acknowledged by the authors. The expertise and financial support of MARIN is also greatly appreciated. In addition, NREL's contribution to this work was supported by the U.S. Department of Energy under Contract No. DE-AC36-08GO28308 with the National Renewable Energy Laboratory. Funding for the work was provided by the DOE Office of Energy Efficiency and Renewable Energy, Wind and Water Power Technologies Office.

## REFERENCES

Bak, C, and Fuglsang, P (2004). "A Method for Deriving 3D Airfoil Characteristics for a Wind Turbine," *Proc 42nd AIAA Aerospace Sciences Meeting and Exhibit*, Reno, Nevada, 291-299.

Buhl Jr., ML (2004). *WT_Perf User's Guide*, National Renewable Energy Laboratory.

Deb, K, Pratap, A, Agarwal, S, and Meyarivan, T (2002). "A Fast and Elitist Multiobjective Genetic Algorithm: NSGA-II," *IEEE Trans Evol Comput*, 6(2), 182-197.

de Ridder, E-J, Otto, W, Zondervan, G-J, Juijs, F, and Vaz, G (2014). "Development of a Scaled-Down Floating Wind Turbine for Offshore Basin Testing," *Proc 33rd ASME Int Conf on Ocean, Offshore and Arctic Eng*, San Francisco, California, 9A, 11pp.

Drela, M (1989). "XFOIL: An Analysis and Design System for Low Reynolds Number Airfoils," *Proc of the Conf on Low Reynolds Number Airfoil Aerodynamics*, University of Notre Dame, 54, 1-12.

Drela, M, and Giles, MB (1987). "Viscous-Inviscid Analysis of Transonic and Low Reynolds Number Airfoils," *AIAA J* **25(10)**.

Fowler, MJ, Kimball, RW, Thomas III, DA, and Goupee, AJ (2013). "Design and Testing of Scale Model Wind Turbines for Use in Wind/Wave Basin Model Test of Floating Offshore Wind Turbines," *Proc 32nd ASME Int Conf on Ocean, Offshore and Arctic Eng*, Nantes, France, 8, 11pp.

Goupee, AJ, and Vel, SS (2007). "Multi-Objective Optimization of Functionally Graded Materials with Temperature-Dependent Material Properties," *Materials and Design* **28**:1861-1879.

Goupee, AJ, Fowler, MJ, Kimball, RW, Helder, J, and de Ridder, E-J (2014). "Additional Wind/Wave Basin Testing of the DeepCwind Semi-Submersible with a Performance-Matched Wind Turbine," *Proc 33rd ASME Int Conf on Ocean, Offshore and Arctic Eng*, San Francisco, California, 9B, 10pp.

Hansen, C (2012). NWTC Design Codes: AirfoilPrep, http://wind.nrel.gov/designcodes/preprocessors/airfoilprep/, accessed August 6, 2012.

Jonkman, JM, and Buhl Jr., ML (2005). *FAST User's Guide,* Tech. Rep., NREL/EL-500-38230, Golden, CO: National Renewable Energy Laboratory.

Kimball, RW, Goupee, AJ, Coulling, AJ, and Dagher, HJ (2012). "Model Test Comparisons of TLP, Spar-Buoy and Semi-Submersible Floating Offshore Wind Turbine Systems," *Proc 2012 SNAME Annual Meeting and Expo*, Providence, Rhode Island, 120, 12pp.

Kimball, RW, Goupee, AJ, Fowler, MJ, de Ridder, E-J, and Helder, J (2014). "Wind/Wave Basin Verification of a Performance-Matched Scale-Model Wind Turbine on a Floating Offshore Wind Turbine Platform," *Proc 33rd ASME Int Conf on Ocean, Offshore and Arctic Eng*, San Francisco, California, 9B, 10pp.

Manwell, JF, Mcgowan, JG, and Rogers, AL (2009). *Wind Energy Explained: Theory, Design and Application, 2nd Ed.*, Chichester: John Wiley & Sons.

Martin, HR, Kimball, RW, Viselli, AM, and Goupee, AJ (2014). "Methodology for Wind/Wave Basin Testing of Floating Offshore Wind Turbines," *J Offshore Mechanics and Arctic Eng* **136(2)**, 021902.

Moriarty, PJ, and Hansen, AC (2005). *AeroDyn Theory Manual*, Tech. Rep., NREL/EL-500-36881, Golden, CO: National Renewable Energy Laboratory.

Pareto, V (1971). *Manual of Political Economy*, New York: A.M. Kelly. Translation of *Manuale di Econimia Politica*, 1906.

APPENDIX A

Round Root Section with a CD of 0.50
Coefficients obtained as documented in ISOPE 2015-TPC-0174

| | |
|---|---|
| 1 | Number of airfoil tables in this file |
| 0 | Table ID parameter |
| 0.0 | No longer used, enter zero |
| 0.0 | No longer used, enter zero |
| 0.0 | No longer used, enter zero |
| 0.0 | Stall angle (deg) |
| 0.0 | Zero Cn angle of attack (deg) |
| 0.0 | Cn slope for zero lift (dimensionless) |
| 0.0 | Cn extrapolated to value at positive stall angle of attack |
| 0.0 | Cn at stall value for negative angle of attack |
| 0.0 | Angle of attack for minimum CD (deg) |
| 0.50 | Minimum CD value |

| | | |
|---|---|---|
| -180 | 0 | 0.5 |
| 0 | 0 | 0.5 |
| 180 | 0 | 0.5 |

MARIN Stock Wind Turbine AG04 Mod Airfoil
Coefficients obtained as documented in ISOPE 2015-TPC-0174

| | |
|---|---|
| 1 | Number of airfoil tables in this file |
| 0 | Table ID parameter |
| 0.0 | No longer used, enter zero |
| 0.0 | No longer used, enter zero |
| 0.0 | No longer used, enter zero |
| 6.00 | Stall angle (deg) |
| -0.7360 | Zero Cn angle of attack (deg) |
| 6.5004 | Cn slope for zero lift (dimensionless) |
| 0.7642 | Cn extrapolated to value at positive stall angle of attack |
| -0.8000 | Cn at stall value for negative angle of attack |
| -0.50 | Angle of attack for minimum CD (deg) |
| 0.0218 | Minimum CD value |

| | | |
|---|---|---|
| -180 | 0.0000 | 0.0625 |
| -170 | 0.4660 | 0.0993 |
| -160 | 0.4280 | 0.2053 |
| -150 | 0.4650 | 0.3674 |
| -140 | 0.4840 | 0.5656 |
| -130 | 0.4620 | 0.7755 |
| -120 | 0.3960 | 0.9710 |
| -110 | 0.2890 | 1.1278 |
| -100 | 0.1520 | 1.2261 |
| -90 | 0.0000 | 1.2530 |
| -80 | -0.1692 | 1.2261 |
| -70 | -0.3193 | 1.1278 |
| -60 | -0.4360 | 0.9710 |
| -50 | -0.5087 | 0.7755 |
| -40 | -0.5350 | 0.5656 |
| -30 | -0.5184 | 0.3674 |
| -20 | -0.4825 | 0.2053 |
| -10 | -0.5208 | 0.0992 |
| -9.0 | -0.5199 | 0.0880 |
| -8.0 | -0.5166 | 0.0765 |
| -7.0 | -0.5100 | 0.0650 |
| -6.0 | -0.4993 | 0.0537 |
| -5.0 | -0.4838 | 0.0428 |
| -4.5 | -0.4277 | 0.0378 |
| -4.0 | -0.3713 | 0.0341 |
| -3.5 | -0.3149 | 0.0310 |
| -3.0 | -0.2584 | 0.0285 |
| -2.5 | -0.2017 | 0.0265 |
| -2.0 | -0.1451 | 0.0249 |
| -1.5 | -0.0883 | 0.0237 |
| -1.0 | -0.0314 | 0.0228 |
| -0.5 | 0.0255 | 0.0218 |
| 0.0 | 0.0824 | 0.0221 |
| 0.5 | 0.1393 | 0.0220 |
| 1.0 | 0.1963 | 0.0221 |
| 1.5 | 0.2532 | 0.0224 |
| 2.0 | 0.3101 | 0.0231 |
| 2.5 | 0.3669 | 0.0239 |
| 3.0 | 0.4237 | 0.0252 |
| 3.5 | 0.4804 | 0.0265 |
| 4.0 | 0.5370 | 0.0282 |
| 4.5 | 0.5935 | 0.0305 |
| 5.0 | 0.6500 | 0.0338 |
| 5.5 | 0.7063 | 0.0382 |
| 6.0 | 0.7625 | 0.0422 |
| 6.5 | 0.7619 | 0.0495 |
| 7.0 | 0.7603 | 0.0625 |
| 7.5 | 0.7579 | 0.0807 |
| 8.0 | 0.7544 | 0.0926 |
| 8.5 | 0.7500 | 0.1019 |
| 9.0 | 0.7456 | 0.1099 |
| 9.5 | 0.7423 | 0.1179 |
| 10 | 0.7410 | 0.1270 |
| 11 | 0.7482 | 0.1482 |
| 12 | 0.7679 | 0.1708 |
| 13 | 0.7970 | 0.1946 |
| 14 | 0.8322 | 0.2191 |
| 15 | 0.8706 | 0.2441 |
| 16 | 0.9090 | 0.2693 |
| 17 | 0.9442 | 0.2943 |
| 18 | 0.9733 | 0.3188 |
| 19 | 0.9930 | 0.3425 |
| 20 | 1.0002 | 0.3650 |
| 25 | 0.9534 | 0.4683 |
| 30 | 0.8794 | 0.5668 |
| 35 | 0.8284 | 0.6597 |
| 40 | 0.7807 | 0.7487 |
| 45 | 0.7354 | 0.8359 |
| 50 | 0.6890 | 0.9183 |
| 60 | 0.5803 | 1.0627 |
| 70 | 0.4187 | 1.1705 |
| 80 | 0.2183 | 1.2351 |
| 90 | 0.0000 | 1.2530 |
| 100 | -0.1520 | 1.2261 |
| 110 | -0.2890 | 1.1278 |
| 120 | -0.3960 | 0.9710 |
| 130 | -0.4620 | 0.7755 |
| 140 | -0.4840 | 0.5656 |
| 150 | -0.4650 | 0.3674 |
| 160 | -0.4280 | 0.2053 |
| 170 | -0.4660 | 0.0993 |
| 180 | 0.0000 | 0.0625 |